# Surface and step magnetic anisotropy

D. S. Chuang, C. A. Ballentine, and R. C. O'Handley
*Massachusetts Institute of Technology, Cambridge, Massachusetts 02139*
(Received 6 October 1993; revised manuscript received 17 February 1994)

Cu(11$n$) surfaces vicinal to Cu(001) are characterized by (001) terraces separated by monoatomic steps. Growth of thin epitaxial magnetic films on such terraced substrates, e.g., Co/Cu(1 1 13), leads to unexpected magnetic anisotropy associated with the surface steps. This anisotropy remains largely unexplained, and is of potential technological importance. We have studied the anisotropy of fcc Co/Cu (1 1 13) films using *in-situ* magneto-optical Kerr effect (MOKE), and find an in-plane uniaxial anisotropy favoring magnetization parallel to the steps. The strength of this anisotropy decreases with increasing film thickness. In this paper we focus on the interpretation of this anisotropy in terms of the Néel model. The Néel anisotropy energy for such a film has the form $E_{\text{film}}=E_{\text{bulk}}-2E_{\text{surface}}/t-2E_{\text{step}}/(td)$, where $t$ and $d$ are film thickness and terrace width, respectively. The last term includes contributions from sites at both the upper edge and inner corner of the step and makes the dominant contribution to the step-induced anisotropy. This model properly accounts for the preferred direction of magnetization parallel to the steps in Co/Cu(1 1 13). bcc Fe/W vicinal to (001) shows a preference for in-plane magnetization perpendicular to the steps for $t<2.5$ monolayers. The Néel model also predicts this anisotropy for a bcc Fe film provided the magnetization lies in the film plane, not in the (001) plane.

## I. INTRODUCTION

Magnetic surface anisotropy (MSA) in epitaxial magnetic thin films and multilayers is a subject of both major technological importance and fundamental scientific interest. Understanding why the magnetization favors a given direction in a materials system is crucial to engineering desired properties in magnetic structures. Many research groups have shown that MSA, including strain effects,[1–4] and effects of substrate morphology,[5–8] is a significant factor governing the anisotropy in films and multilayers. In some systems, the MSA is strong enough to overcome the magnetostatic energy of the film and produce a perpendicular easy axis [e.g., Ni/Cu (Ref. 2), Fe/Ag (Ref. 9), Fe/Cu (Ref. 10)]. Interpretations of surface anisotropy have focused largely on phenomenological descriptions using the Néel surface anisotropy model.[11,12] There have been a few first-principles calculations. Recently, Victora and MacLaren have worked to bring these two approaches together, demonstrating that the Néel model gives good agreement to electronic structure calculation results as well as to experimental results for Co/Pd multilayers.[1] They also demonstrated the importance of taking the strain effects into account in the Néel model for that system.

In an effort to more fully understand MSA, a few groups are investigating the anisotropy in magnetic films grown on well-defined, stepped substrates. The stepped morphology is obtained either by using a vicinal surface, cut slightly off a low index crystal plane, or by carefully controlling growth conditions in order to create surface steps. The systems studied include fcc Co/Cu vicinal to (001),[6,7,13] bcc Fe/W vicinal to (001),[8] and bcc Fe/W stepped (110).[5] Albrecht *et al.*[5] have shown that the main aspects of the step-induced anisotropy in Fe/W stepped (110) can be explained by Néel's model. Here we focus on the Co/Cu vicinal to (001) system.

Stable Cu surfaces vicinal to (001) are of the type (11$n$), and are characterized by (001) terraces $n/2$ atoms wide.[14] The terraces are separated by monoatomic steps perpendicular to the [110] direction (see Fig. 1). Co films grown epitaxially on such a substrate exhibit a step-induced uniaxial magnetic anisotropy which favors **M** parallel to the steps.[6,7,13]

In this paper, we present a full treatment of the Néel anisotropy in Co/Cu vicinal to (001) surfaces. Our treatment describes the anisotropy in this materials system due to broken or missing bonds at the surface and step edges, as well as the strains in the remaining bonds. Our model predicts the experimentally observed orientation of the easy axis in the Co/Cu(11$n$) system, and gives reasonable agreement with the magnitude of the measured anisotropies. It also predicts the observed anisotropy in a similarly stepped system Fe/W vicinal to (001).[8]

## II. NÉEL SURFACE ANISOTROPY MODEL

Néel proposed that atoms in an environment of reduced symmetry, such as those at a surface, will give rise to anisotropies that are different from the bulk anisotropy in the material. In the Néel model, the magnetic pair-interaction energy between atoms is expanded in Legendre polynomials:[11]

$$w(r,\psi)=G(r)+L(r)(\cos^2\psi-\tfrac{1}{3})+Q(r)(\cos^4\psi-\tfrac{6}{7}\cos^2\psi-\tfrac{3}{35})+\cdots . \quad (1)$$

This interaction depends on $\psi$, the angle between the bond axis and $\mathbf{M}_s$, and on the distance between the pair of atoms $r$ [see Fig. 2(a)]. The first term, which is independent of $\psi$, includes the spatially isotropic effects such as magnetic exchange $E_{\text{ex}}=-J_{ij}S_i\cdot S_j$. It does not

 

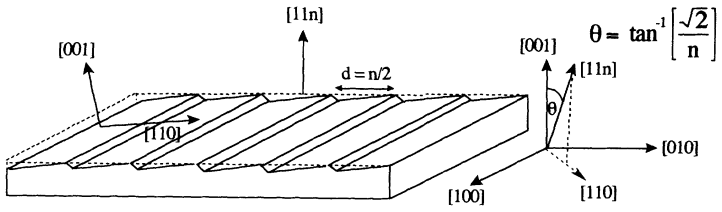


FIG. 1. Schematic of an ideal Cu(11$n$) surface characterized by (001) terraces separated by atomic steps parallel to [1$\underline{1}$0]. The terraces are $d=n/2$ atoms wide.

contribute to magnetic anisotropy. The second, dipolar term describes anisotropies with a twofold axis. The third, quadrupolar term describes anisotropy of cubic symmetry. We calculate the magnetic anisotropy energy of a film by summing this interaction energy $w(r,\psi)$ for all pairs of atoms in the film.

Strain is present in ultrathin films for various reasons, such as surface relaxation[15] and film/substrate misfit.[16] Anisotropy due to these strains is described via the Néel model by taking into account the strain-induced changes in $r$ and $\psi$.[17] The coefficients of Eq. (1) are functions of the distance $r$ between the pairs of magnetic atoms, and can be expanded in terms of the bond strain

$$L_i(r)=L_i(r_0)+(dL_i/dr)\cdot\mathbf{e}\cdot r_0+\cdots, \tag{2}$$

where $r_0$ is the bulk unstrained bond length. The subscript indicates the type of interaction being considered, (e.g., $i=1$ denotes an interaction between first-nearest neighbors, $i=2$ denotes a second-nearest-neighbor interaction). For a given material, the values of $L_i(r_0)$ and $Q_i(r_0)$, as well as their variation with the bond length [e.g., $(dL_i/dr)r_0$] can be related to the anisotropy constant $K_1$, and the magnetoelastic coefficients $B_1$ and $B_2$ of the bulk material.[17] Because we cannot separate first-nearest- and second-nearest-neighbor effects in the definition of $B_1$ and $B_2$, and because the interaction strength should decrease with bond length, we assume that second-nearest-neighbor interactions are relatively insignificant. We have calculated the Néel coefficients for fcc Co using $K_1$, $B_1$, and $B_2$ values extrapolated from the data of Fujiwara, Kadomatsu, and Tokaunaga taken at 4 K.[18] These coefficients are listed in Table I along with the coefficients for bcc Fe, as dictated by bulk magnetic parameters.[19] We have dropped the subscript $i=1$ for convenience. As seen in Table I, the magnitude of $L(r_0)$ is two orders of magnitude larger than $Q(r_0)$; therefore, we neglect the quadrupole, and higher-order terms of Eq. (1) in all cases where the dipole term contributes to the anisotropy.

The Néel coefficients can alternatively be determined using first-principles calculations, as done by Victora and MacLaren.[1] We note that the values of $L(r_0)$ and $(dL/dr)r_0$ given in Table I predict an $L(r)$ for Co-Co interactions at a bond separation r as found in Co/Pd multilayers[1] that is within 6% of the value obtained from the electronic structure calculations of Victora and MacLaren for that system.

We describe the strain in the bonds around a given atom by a strain tensor given in the low index surface coordinate system, as defined in Tables II, III, and IV:

$$e=\begin{bmatrix} e_{xx} & e_{xy} & e_{xz} \\ e_{xy} & e_{yy} & e_{yz} \\ e_{xz} & e_{yz} & e_{zz} \end{bmatrix}. \tag{3}$$

For the calculations presented in this paper, we consider a biaxial strain that is uniform throughout the thickness of the film, such as that due to unrelieved misfit between the film and substrate. The misfit strain in the film has the form

$$e=e_0\begin{bmatrix} 1 & 0 & 0 \\ 0 & 1 & 0 \\ 0 & 0 & \dfrac{-2\nu}{1-\nu} \end{bmatrix}. \tag{4}$$

$e_0$ is the misfit $e_0=(a_{\text{substrate}}-a_{\text{film}})/a_{\text{substrate}}$, and Poisson's ratio ($\nu$) is assumed to be $\frac{1}{3}$.

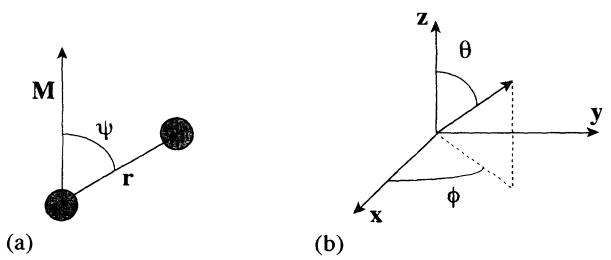


FIG. 2. (a) The angle $\psi$ between $\mathbf{M}_s$ and the bond axis, r. (b) $\theta$ and $\phi$, the angles used to define the direction of a vector (e.g., $\mathbf{M}_s$) with respect to the coordinate axes.

## III. NÉEL'S MODEL APPLIED TO (11$n$) STEPPED FILMS

For Co/Cu(11$n$) films we can identify four distinct types of atomic sites in the film which are indicated in Fig. 3(a): bulk, surface, step-edge, and step-corner sites. Each type of site contributes in a different way to the magnetic anisotropy. Bulk fcc Co atoms have twelve nearest neighbors, as shown in Fig. 3(b). The symmetry of a surface site is reduced compared to that of the bulk because four nearest-neighbor bonds are broken in the creation of the surface. These bonds are along [011], [0$\underline{1}$1], [101], and [$\underline{1}$01] directions. The resulting nearest-neighbor cluster around a surface atom contains only eight atoms [Fig. 3(c)].

In creating the surface steps parallel to [1$\underline{1}$0] in

TABLE I. Anisotropy constant $K_1$ and magnetoelastic coefficients $B_1$, $B_2$ for fcc Co (at 4 K) and bcc Fe (at 298 K), and the Néel model parameters derived from them.

| | $K_1$ $10^6$ erg/cm$^3$ | $Q(r_0)$ $10^6$ erg/cm$^3$ | $B_1$ $10^8$ erg/cm$^3$ | $B_2$ $10^8$ erg/cm$^3$ | $L(r_0)$ $10^8$ erg/cm$^3$ | $(dL/dr)\ r_0$ $10^8$ erg/cm$^3$ |
|---|---|---|---|---|---|---|
| fcc Co | −1.2 | −1.2 | −1.6 | 2.6 | −1.5 | 5.5 |
| bcc Fe | 0.47 | 0.26 | −0.29 | 0.71 | −0.11 | 0.91 |

Cu(11$n$), three additional bonds are broken. One of these is between the atom at the upper edge of the step and its nearest neighbor in the [110] direction; leaving the edge-site atom with only seven nearest neighbors [Fig. 3(d)]. The other two broken bonds are associated with atoms formerly in bulk sites, but now at the inner corner of the step. These bonds are along [101] and [011] directions. The corner-site atom is left with ten nearest neighbors [Fig. 3(e)].

The anisotropy contributions to each of the reduced symmetry sites (e.g., surface, and step sites) can be determined in either of two ways. We can sum the energies of the bonds present in the nearest-neighbor clusters, or alternatively, we can sum the energies of the broken bonds and subtract this sum from the anisotropy energy of a bulk cluster. Both methods lead to the same result for the magnetic anisotropy of the entire film. We use the latter. The anisotropy energy density for the film is then given by

$$E_{\text{film}}=E_{\text{bulk}}-2\frac{E_{\text{surface}}}{t}-2\frac{(E_{\text{step edge}}+E_{\text{step corner}})}{td}\ , \quad (5)$$

where $E_{\text{bulk}}$, $E_{\text{surface}}$, $E_{\text{step edge}}$, and $E_{\text{step corner}}$ are in units of energy/volume, energy/area, energy/length, and energy/length, respectively. $t$ and $d$ are the film thickness and the terrace width, respectively. [See the Appendix for a derivation of Eq. (5).] Equation (5) indicates, as expected, that as the film thickness increases, anisotropy effects from the surface and steps will become less important. Similarly, in systems with wider terraces, step effects will not be as significant.

## IV. IMPORTANCE OF STRAIN EFFECTS

To illustrate the importance of the magnetoelastic effects due to misfit strain, we compare the anisotropy energy for unstrained bulk fcc Co with that for bulk cobalt strained by the Co/Cu misfit $e_0=1.9\%$ ($a_{\text{Co}}=0.3546$ nm, $a_{\text{Cu}}=0.3615$ nm). The forms of these energies, obtained from Eq. (1) and Eq. (2) are

$$E_{\text{bulk}}^{\text{unstrained}}=\frac{Q(r)}{4}(\sin^2 2\theta+\sin^2 2\phi\sin^4\theta)=E_{\text{MC}} \quad (6)$$

for the unstrained fcc bulk, and

$$E_{\text{bulk}}^{\text{strained}}=e_0\left[6L(r_0)+\frac{dL}{dr}r_0\right]\sin^2\theta+E_{\text{bulk}}^{\text{unstrained}} \quad (7)$$

for the strained fcc bulk. $\theta$ and $\phi$ are defined in Fig. 2(b), where $\mathbf{x}=[100]$, $\mathbf{y}=[010]$, and $\mathbf{z}=[001]$ for this system.

In the unstrained case, Eq. (6), the dipole terms have

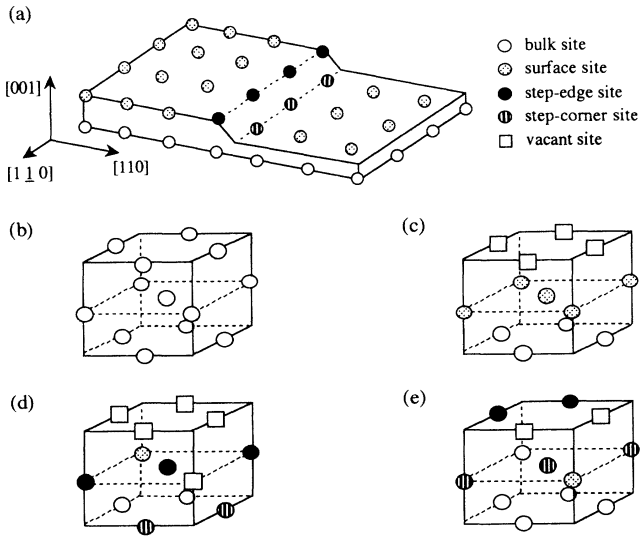


FIG. 3. (a) Region around a surface step in Co/Cu(11$n$), sites of different symmetry are indicated. Nearest-neighbor clusters are shown for (b) bulk fcc Co sites, (c) surface sites, (d) step-edge sites, and (e) step-corner sites.

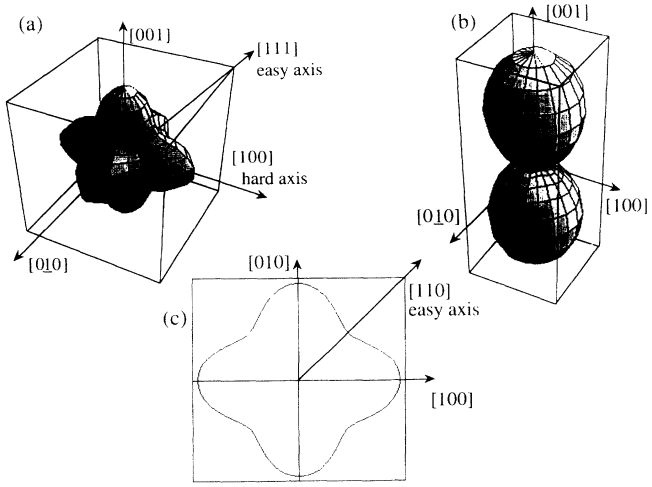


FIG. 4. (a) Anisotropy energy surface for unstrained fcc Co bulk. (b) Anisotropy surface energy for fcc Co bulk strained by the 1.9% misfit between Co and Cu induced by epitaxial growth on Cu. (c) An (001) cut through the strained bulk's energy surface showing the presence of fourfold anisotropy in the (001) plane.

cancelled upon the summation over nearest neighbors. The resulting anisotropy is simply the magnetocrystalline anisotropy, $E_{MC}$, where the anisotropy constant $K_1=Q(r)$, (i.e., the angular term is identical to $\alpha_1^2\alpha_2^2+\alpha_2^2\alpha_3^2+\alpha_1^2\alpha_3^2$). Figure 4(a) shows the form of this energy surface; a constant has been added so that its shape can be seen more clearly. It exhibits the expected form for magnetic anisotropy in a cubic material with $K_1<0$. The $\langle 111 \rangle$ directions are magnetically easy.

After the symmetry around a bulk atom is reduced by misfit strain, the dipole effects no longer balance each other. The importance of the dipole term which remains in the strained case, Eq. (7), is illustrated in Fig. 4(b). Magnetoelastic effects give rise to a strong uniaxial anisotropy which favors **M** in the plane of the film. The difference in energy between **M** out of the plane (along [001]) and **M** in plane (along [100]) changes from $\Delta E=0$ in the unstrained case to $\Delta E\sim 10^7$ erg/cm$^3$ ($7\times 10^{-5}$ eV/atom) in the strained case. This adds to the effect of the magnetostatic energy ($\Delta E_{MS}\sim 10^7$ erg/cm$^3$) which also works to bring the magnetization in plane. In Fig. 4(c) we show the anisotropy energy in a (001) plane cross section of the surface in Fig. 4(b) to demonstrate that in the presence of strain, there is still fourfold symmetry about the [001] axis. The magnetic easy directions in the (001) surface of the strained bulk are still the $\langle 110 \rangle$ directions. The anisotropy in the (001) plane is $3\times 10^5$ erg/cm$^3$, very small relative to the strain-induced anisotropy.

The presence of any strain in the film will similarly affect the surface and step anisotropies. Strain contributions alter the unstrained surface and step anisotropies in Co/Cu(11$n$) ($e_0=1.9\%$) by approximately 12% and 8%, respectively. These contributions scale with the misfit strain.

## V. ANISOTROPY IN Co/Cu(1 1 13)

We have used the Néel model to calculate the anisotropy energies $E_{bulk}$ and $E_{surface}$ for simple- (sc), body-centered- (bcc), and face-centered- (fcc) cubic structures with low index surfaces, as well as $E_{step\ edge}$, and $E_{step\ corner}$ for fcc(001) and bcc(001) vicinal surfaces. In order to obtain these results, we incorporated the Néel model in a MATHEMATICA® program with which we can calculate and plot $E(\theta,\phi)$ for any cluster of atoms in the presence of any strain described by Eq. (3). The expressions for anisotropy energies in (001), (110), and (111) systems are given in Tables II, III, and IV, respectively. Upon summation of the interaction energy over nearest neighbors, the angle $\psi$ has been written in terms of $\theta$ and $\phi$ (Fig. 2). The surface and bulk anisotropy energies in the tables correspond to those calculated by Victora and MacLaren for the unstrained case ($e_0=0$) upon an appropriate rotation of the coordinate system. We present each energy in a coordinate system in which z is along the surface normal, as described in the tables.

Figures 5–8 illustrate the calculated results for the strained Néel anisotropy in fcc Co/Cu(11$n$). For each type of site described in Sec. III, we show the anisotropy energy surface, and the cross sections of this surface for the (001) and (1 1 13) planes. These cross sections depict the in-plane anisotropy due to each particular site. We are concerned with the in-plane anisotropy because the strong magnetostatic energy ($2\pi M_s^2\sim 10^7$ erg/cm$^3$ $\sim 7\times 10^{-5}$ eV/atom for fcc Co) works to confine **M** in the plane of the film. A measure of the in-plane uniaxial anisotropy, $\Delta E_{\parallel\text{-}\perp}$, is defined as the energy difference between **M** parallel to the steps ($\phi=-\pi/4$) and **M** perpendicular to the steps ($\phi=\pi/4$). The negative of the surface and step-site contributions to the anisotropy energy is displayed so that a minimum in the site energy surfaces corresponds to a minimum for that site's contribution to the total film anisotropy energy as described by Eq. (5). We note that only the dipole effects are shown below, but the bulk quadrupole, or magnetocrystalline, anisotropy effects (Fig. 4) should not be neglected when considering the total anisotropy of the film.

The anisotropy contribution due to the strained bulk is shown in Fig. 5(a), with the anisotropy in (001) and (1 1 13) plane cross sections of this surface in Fig. 5(b). In the (001) surface, as shown with the dotted lines, the energy is constant and there is no in-plane anisotropy. Upon rotation into the (1 1 13) plane, the surface is no longer perpendicular to a high symmetry axis of the energy surface. This reduction in symmetry results in uniaxial in-plane anisotropy with the [1$\underline{1}$0] direction parallel to the steps ($\phi=\pi/4,3\pi/4$) being easier than the step normal ($\Delta E_{\parallel\text{-}\perp,bulk}=-7\times 10^4$ erg/cm$^3$ $=-5\times 10^{-7}$ eV/atom).

The anisotropy energy corresponding to bonds broken to create the surface is shown in Fig. 6. This contribution also favors **M** in the plane of the film, reinforcing the effects of magnetostatic energy and the bulk anisotropy contribution in the strained film. The (001) cross section of this energy surface reveals that there is no (001) in-plane anisotropy associated with surface sites. For **M** confined to the (1 1 13) plane, however, the surface anisotropy contribution favors magnetization parallel to the steps ($\Delta E_{\parallel\text{-}\perp,surface}=-0.013$ erg/cm$^2$ $=-5\times 10^{-6}$ eV/atom). Again, this uniaxial anisotropy is simply a consequence of the fact that unlike the (001) plane, the (1 1 13) plane is not perpendicular to the symmetry axis of the energy surface.

The contribution from the upper-step-edge site is shown in Fig. 7. The anisotropy due to this site favors **M** in the (1$\underline{1}$0) plane, which is parallel to the steps. The reduced symmetry at this site contributes a strong uniaxial in-plane anisotropy when **M** is confined in either the (001) or (1 1 13) plane. The energy difference $\Delta E_{\parallel\text{-}\perp,step\ edge}$ in both of these planes is quite large, approximately $-2.9\times 10^{-8}$ erg/cm ($-7\times 10^{-5}$ eV/atom) favoring magnetization parallel to the steps.

The inner-step-corner site contributes the anisotropy energy illustrated in Fig. 8. The (001) cross section of this surface reveals that there is no in-plane magnetic anisotropy due to this site. In the (1 1 13) plane, however, **M** perpendicular to the steps is favored by $\Delta E_{\parallel\text{-}\perp,step\ corner}=0.47\times 10^{-8}$ erg/cm $=1\times 10^{-5}$ eV/atom. As seen by comparing Fig. (7) and Fig. (8), the two step-site contributions counteract one another in the (1 1 13) plane, but the much stronger upper-step-edge

TABLE II. Bulk, (001) surface, and step anisotropy energies for cubic structures in the (001) surface coordinate system: $\mathbf{x}=[100]$, $\mathbf{y}=[010]$, $\mathbf{z}=[001]$. As in the Appendix, $h$ and $w$ are the height of a monolayer and the distance between terrace atoms, respectively.

| (001) system | Anisotropy energy $\mathbf{x}=[100]$, $\mathbf{y}=[010]$, $\mathbf{z}=[001]$ |
|---|---|
| Bulk, unstrained | $E_{\text{bulk}}^{\text{unstrained}}\left[\frac{\text{erg}}{\text{cm}^3}\right]=E_{\text{MC}}$ |
| Simple cubic (sc) | $\frac{-Q(r_0)}{2}(\sin^2 2\theta+\sin^2 2\phi\sin^4\theta)$ |
| Body-centered cubic (bcc) | $\frac{4Q(r_0)}{9}(\sin^2 2\theta+\sin^2 2\phi\sin^4\theta)$ |
| Face-centered cubic (fcc) | $\frac{Q(r_0)}{4}(\sin^2 2\theta+\sin^2 2\phi\sin^4\theta)$ |
| Bulk, strained | $E_{\text{bulk}}^{\text{strained}}\left[\frac{\text{erg}}{\text{cm}^3}\right]$ |
| sc | $-2e_0\frac{dL}{dr}r_0\cos^2\theta$ |
| bcc | $-\frac{16}{3}e_0L(r_0)\cos^2\theta$ |
| fcc | $-\left[6e_0L(r_0)+e_0\frac{dL}{dr}r_0\right]\cos^2\theta$ |
| Surface | $\frac{1}{h}E_{\text{surface}}\left[\frac{\text{erg}}{\text{cm}^3}\right]$ |
| sc(001) | $\frac{1}{2}\left[e_0\frac{dL}{dr}r_0+L(r_0)\right]\cos^2\theta$ |
| bcc(001) | $-\frac{8}{3}L(r_0)e_0\cos^2\theta$ |
| fcc(001) | $\left[\frac{L(r_0)}{2}-3e_0L(r_0)\right]\cos^2\theta$ |
| Step | $\frac{1}{wh}E_{\text{step site}}\left[\frac{\text{erg}}{\text{cm}^3}\right]$ |
| bcc(001) with steps $\parallel[100]$ | |
| $E_{\text{step edge}}$ | 0 |
| $E_{\text{step corner}}$ | $-\frac{4}{3}L(r_0)e_0\cos^2\theta+\left[\frac{2}{3}L(r_0)-\frac{4}{9}e_0L(r_0)+\frac{2}{9}e_0\frac{dL}{dr}r_0\right]\sin\phi\cos\theta\sin\theta$ |
| fcc(001) with steps $\parallel[1\bar{1}0]$ | |
| $E_{\text{step edge}}$ | $-\frac{1}{4}\left[L(r_0)+e_0\frac{dL}{dr}r_0\right]\cos^2\theta+\frac{1}{2}\left[L(r_0)+e_0\frac{dL}{dr}r_0\right]\sin\phi\cos\phi\sin^2\theta$ |
| $E_{\text{step corner}}$ | $\left[\frac{1}{4}L(r_0)-\frac{3}{2}e_0L(r_0)\right]\cos^2\theta+\frac{1}{2}L(r_0)\cos\theta\sin\theta(\sin\phi+\cos\phi)$ |

effect dominates giving a combined step effect which always favors **M** parallel to the steps for Co/Cu($11n$) with $\Delta E_{\parallel\text{-}\perp,\text{step}}=-2.4\times10^{-8}$ erg/cm $=-6\times10^{-5}$ eV/atom.

The Néel anisotropy of the film is obtained by substituting the four contributions described above into Eq. (5). In Co/Cu(1 1 13) films, the energy difference $\Delta E_{\parallel\text{-}\perp,\text{film}}$ is given by

$$\Delta E_{\parallel\text{-}\perp,\text{film}}=\left[-0.7-\frac{190}{t_{\text{ML}}}\right]\times10^5\ \text{erg/cm}^3\ , \tag{8}$$

where $t_{\text{ML}}$ is the thickness of the film in monolayers. Magnetization parallel to the steps is always favored

TABLE III. Bulk and (110) surface energies for cubic structures in the (110) surface coordinate system: x=[1$\underline{1}$0], y=[00$\underline{1}$], z=[110]. $h$ is the height of a monolayer in cm.

| (110) System | Anisotropy energy x=[1$\underline{1}$0], y=[00$\underline{1}$], z=[110] |
|---|---|
| Bulk, strained | $E_{\text{bulk}}^{\text{strained}}\left[\frac{\text{erg}}{\text{cm}^3}\right]$ |
| sc | $-\left[2e_0L(r_0)+e_0\frac{dL}{dr}r_0\right]\cos^2\theta+\left[2e_0L(r_0)-e_0\frac{dL}{dr}r_0\right]\cos^2\phi\sin^2\theta$ |
| bcc | $-\left[\frac{32}{9}e_0L(r_0)+\frac{8}{9}e_0\frac{dL}{dr}r_0\right]\cos^2\theta+\left[-\frac{16}{9}e_0L(r_0)+\frac{8}{9}e_0\frac{dL}{dr}r_0\right]\cos^2\phi\sin^2\theta$ |
| fcc | $-\left[5e_0L(r_0)+\frac{3}{2}e_0\frac{dL}{dr}r_0\right]\cos^2\theta+\left[-e_0L(r_0)+\frac{1}{2}e_0\frac{dL}{dr}r_0\right]\cos^2\phi\sin^2\theta$ |
| Surface | $\frac{1}{h}E_{\text{surface}}\left[\frac{\text{erg}}{\text{cm}^3}\right]$ |
| sc(110) | $\left[\frac{1}{2}L(r_0)-e_0L(r_0)\right]\cos^2\theta+\left[\frac{1}{2}L(r_0)+e_0L(r_0)\right]\cos^2\phi\sin^2\theta$ |
| bcc(110) | $\left[\frac{1}{3}L(r_0)-\frac{16}{9}e_0L(r_0)-\frac{1}{9}e_0\frac{dL}{dr}r_0\right]\cos^2\theta-\left[\frac{1}{3}L(r_0)+\frac{8}{9}e_0L(r_0)-\frac{1}{9}e_0\frac{dL}{dr}r_0\right]\cos^2\phi\sin^2\theta$ |
| fcc(110) | $\left[\frac{1}{2}L(r_0)-\frac{5}{2}e_0L(r_0)-\frac{5}{4}e_0\frac{dL}{dr}r_0\right]\cos^2\theta-\left[\frac{1}{2}L(r_0)+\frac{1}{2}e_0L(r_0)+\frac{1}{4}e_0\frac{dL}{dr}r_0\right]\cos^2\phi\sin^2\theta$ |

TABLE IV. Bulk and (111) surface energies for cubic structures in the (111) surface coordinate system: x=[11$\underline{2}$], y=[$\underline{1}$10], z=[111]. $h$ is the height of a monolayer in cm.

| (111) System | Anisotropy energy x=[11$\underline{2}$], y=[$\underline{1}$10], z=[111] |
|---|---|
| Bulk, strained | $E_{\text{bulk}}^{\text{strained}}\left[\frac{\text{erg}}{\text{cm}^3}\right]$ |
| sc | $-4e_0L(r_0)\cos^2\theta$ |
| bcc | $-\frac{16}{9}\left[e_0L(r_0)+e_0\frac{dL}{dr}r_0\right]\cos^2\theta$ |
| fcc | $-\left[4e_0L(r_0)+2e_0\frac{dL}{dr}r_0\right]\cos^2\theta$ |
| Surface | $\frac{1}{h}E_{\text{surface}}\left[\frac{\text{erg}}{\text{cm}^3}\right]$ |
| sc(111) | $-2e_0L(r_0)\cos^2\theta$ |
| bcc(111) | $\left[\frac{1}{2}L(r_0)-\frac{8}{9}e_0L(r_0)-\frac{25}{18}e_0\frac{dL}{dr}r_0\right]\cos^2\theta$ |
| fcc(111) | $\left[\frac{3}{4}L(r_0)-2e_0L(r_0)-\frac{1}{4}e_0\frac{dL}{dr}r_0\right]\cos^2\theta$ |

($\Delta E_{\parallel\text{-}\perp,\text{film}}<0$), but the magnitude of $\Delta E_{\parallel\text{-}\perp,\text{film}}$ decreases with increasing film thickness, as shown in Fig. 9. Even for $t_{\text{ML}}\rightarrow\infty$ there is a weak uniaxial anisotropy parallel to the steps in an fcc film on a (11$n$) vicinal surface.

We compare this predicted strength of the in-plane uniaxial anisotropy to that measured on Co/Cu(1 1 13) films of various thicknesses. In-plane anisotropies have been measured on 14-ML and 20-ML films, as shown in Fig. 9. Thinner films of 2 ML,[20] 3 ML,[13] 6 ML,[21] and 10 ML (Ref. 20) thickness have also been studied, but the hard axis, perpendicular to the steps, could not be saturated with the fields available *in situ*. The solid line is the behavior indicated in Eq. (8). The Néel model clearly predicts the correct orientation of the easy axis: parallel to the steps. The measured strength of the in-plane anisotropy is smaller than that predicted. For example, in the 14-ML film, the measured value, $\Delta E_{\parallel\text{-}\perp}^{\text{experimental}}=-3\times10^5$ erg/cm$^3$ is approximately five times smaller than the anisotropy calculated using the model: $\Delta E_{\parallel\text{-}\perp,\text{film}}=-14\times10^5$ erg/cm$^3$. Our measurements were made at room temperature and the calculated values were based on low-temperature parameters (Table I).

If we consider only the bulk and surface contributions to the anisotropy in the 14-ML (1 1 13) film, we predict $\Delta E_{\parallel\text{-}\perp,\text{film}}=-1.7\times10^5$ erg/cm$^3$. Because we observe an anisotropy stronger than this, but not as strong as that calculated for perfect steps, it appears that step effects are

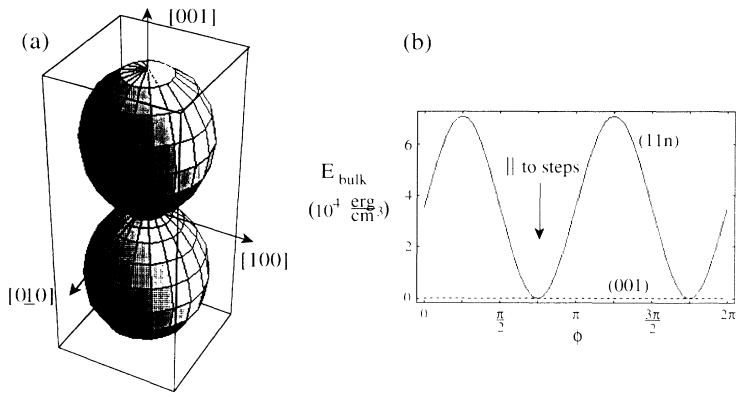


FIG. 5. (a) Anisotropy energy surface for a bulk site in a fcc Co(11$n$) film. (b) In-plane anisotropy for (001) and (1 1 13) planes through this energy surface. (001) anisotropy is shown as a dotted line, (1 1 13) anisotropy as a solid line. The surface steps are along [1$\underline{1}$0], defined by $\phi = 3\pi/4, 7\pi/4$.

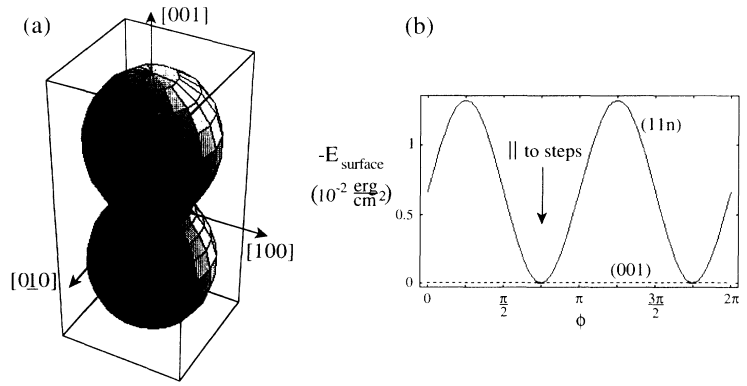


FIG. 6. (a) Anisotropy energy surface for the surface site in a fcc Co(11$n$) film. (b) In-plane anisotropy for (001) and (1 1 13) planes through this surface. (001) anisotropy is shown as a dotted line, (1 1 13) anisotropy as a solid line. The surface steps are along [1$\underline{1}$0], defined by $\phi = 3\pi/4, 7\pi/4$.

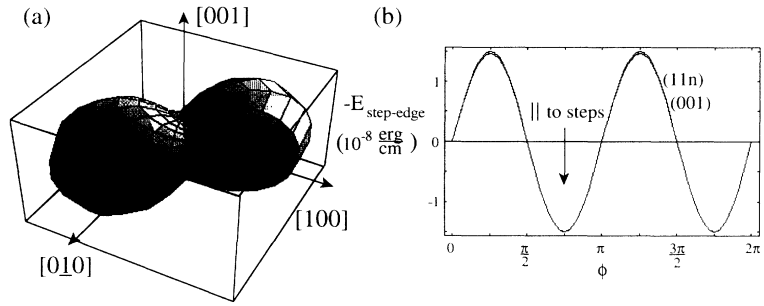


FIG. 7. (a) Anisotropy energy surface for the step-edge site in a fcc Co(11$n$) film. (b) In-plane anisotropy for (001) and (1 1 13) planes through this surface. (001) anisotropy is shown as a dotted line, (1 1 13) anisotropy as a solid line. The surface steps are along [1$\underline{1}$0], defined by $\phi = 3\pi/4, 7\pi/4$.

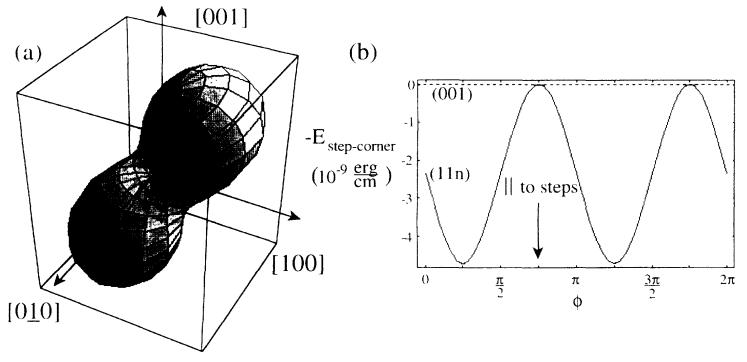


FIG. 8. (a) Anisotropy energy surface for the step-corner site in a fcc Co(11$n$) film. (b) In-plane anisotropy for (001) and (1 1 13) planes through this surface. (001) anisotropy is shown in a dotted line, (1 1 13) anisotropy is in a solid line. The surface steps are along [1$\underline{1}$0], defined by $\phi = 3\pi/4, 7\pi/4$.

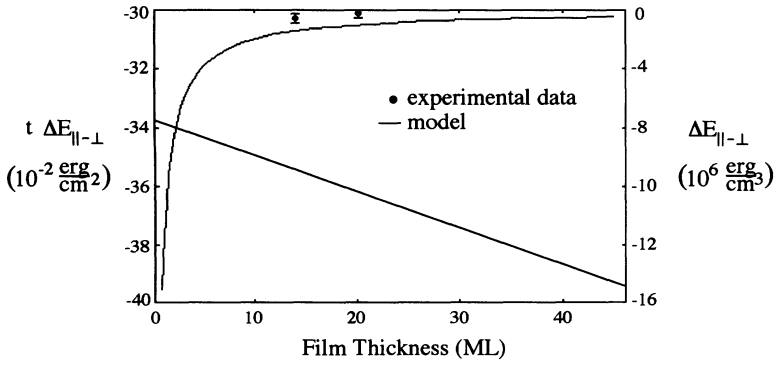


FIG. 9. Calculated strength of the uniaxial anisotropy in Co/Cu(1 1 13) films as a function of film thickness. The straight line is the anisotropy energy times the film thickness (left scale), while the curve is the anisotropy energy (right scale). Experimentally measured anisotropies are shown for 14- and 20-ML films (right scale).

contributing to the experimentally observed anisotropy, but not to the extent that we predict for an ideal stepped surface. The discrepancy may be accounted for by considering that the steps are roughened.

Our model predicts that while very thin films show strong uniaxial anisotropy, the anisotropy of thicker Co/Cu(11$n$) films will approach the biaxial in-plane anisotropy found in Co/Cu(001). This transition from uniaxial to biaxial behavior occurs because the effects of the steps weaken as film thickness increases, as described in Eq. (5). We used $d^2E/d\phi^2$, the curvature of the in-plane anisotropy energy, evaluated at $\phi=\pi/4$ (perpendicular to the steps), to characterize this transition. As shown in Fig. 10, for Co/Cu(1 1 13) films thinner than 17 monolayers this curvature is negative indicating that perpendicular to the steps is a hard axis. For thicknesses greater than 17 ML, the curvature is positive, and the direction perpendicular to the steps is a local minimum for the in-plane anisotropy energy. We note, however, that parallel to the steps remains the global minimum, as previously indicated in Fig. 9.

## VI. ANISOTROPY IN Fe/W VICINAL TO (001)

We have also applied our model to bcc Fe/W vicinal to (001) which was studied by Chen and Erskine.[8] The normal to their vicinal surface is 4° from the [001] direction toward [010] making the Miller indices of the surface (01$n$) where $n$ is $1/\tan(4°)$, or approximately (0 1 14). This vicinal W surface is characterized by 2.5-nm wide (001) terraces separated by atomic steps parallel to [100], and the lattice mismatch between bcc Fe ($a_{Fe}=0.2866$ nm) and W ($a_W=0.3165$ nm) is 9.4%. Fe films grown on such a surface are magnetized in-plane with an easy axis *perpendicular* to the steps for thicknesses between 1 and 2.5 ML.[8]

As in Co/Cu(11$n$) films, the Fe/W vicinal to (001) films contain four types of atomic sites: bulk, surface, step edge, and step corner (see Fig. 11). In a bcc(001) system the step-edge sites and surface sites have the same arrangement of nearest neighbors. Upon creation of surface steps parallel to [100] in a bcc (001) surface, no nearest-neighbor bonds need to be broken around the step-edge atoms. Therefore, as indicated in Table II, there is no step-edge contribution to the anisotropy.

The bulk contribution to the anisotropy in the stepped Fe films is shown in Fig. 12. As in the treatment of Co/Cu, we do not show the magnetocrystalline anisotropy of the bulk bcc structure, although it should not be neglected in the treatment of the anisotropy in the film. Because of the misfit strain, described in Eq. (4) with $e_0=9.4\%$, the bulk anisotropy favors magnetization in the (001) plane. For **M** in the (001) plane, there is no in-plane anisotropy, as shown by the dotted line. In the

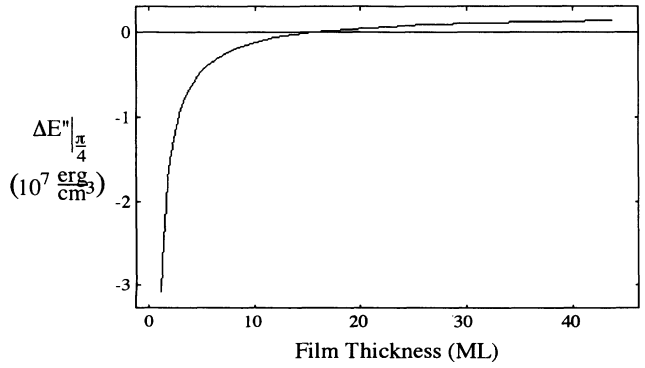


FIG. 10. The calculated transition from uniaxial to biaxial anisotropy with increasing film thickness in Co/Cu(1 1 13) films. $\Delta E''$ is $d^2E/d\phi^2$ and has been evaluated at $\phi=\pi/4$, the direction perpendicular to the steps.

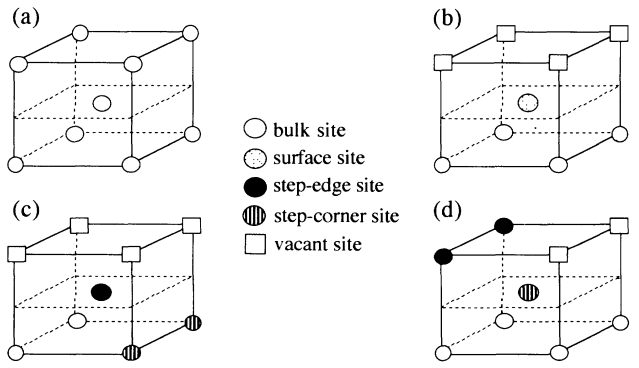


FIG. 11. Nearest-neighbor clusters for (a) bulk bcc Fe sites, (b) surface sites, (c) step-edge sites, and (d) step-corner sites. The nearest-neighbor clusters around surface and step-edge sites are the same with only four nearest neighbors.

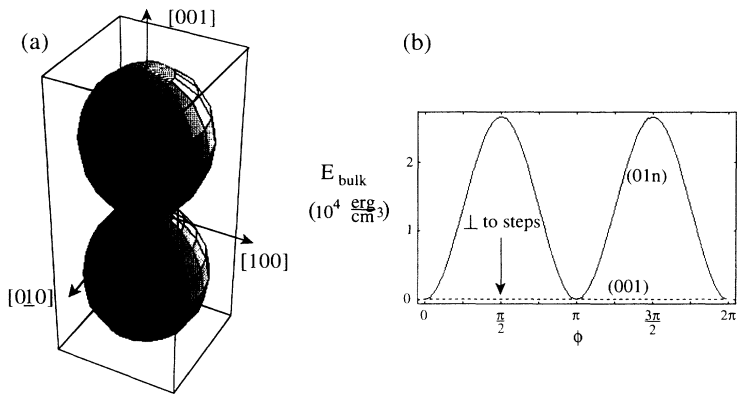


FIG. 12. (a) Anisotropy energy surface for a bulk site in a bcc Fe (01$n$) film, and (b) in-plane anisotropy for (001) and (0 1 14) planes through this surface. (001) anisotropy is shown as a dotted line, (0 1 14) anisotropy as a solid line. The surface steps are along [100], defined by $\phi=0,\pi$.

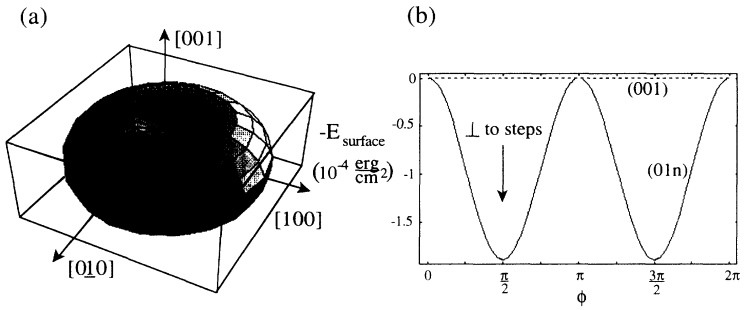


FIG. 13. (a) Anisotropy energy surface for a surface site in a bcc Fe (01$n$) film. (b) In-plane anisotropy for (001) and (0 1 14) planes through this surface. (001) anisotropy is shown in a dotted line, (0 1 14) anisotropy is in a solid line. The surface steps are along [100], defined by $\phi=0,\pi$.

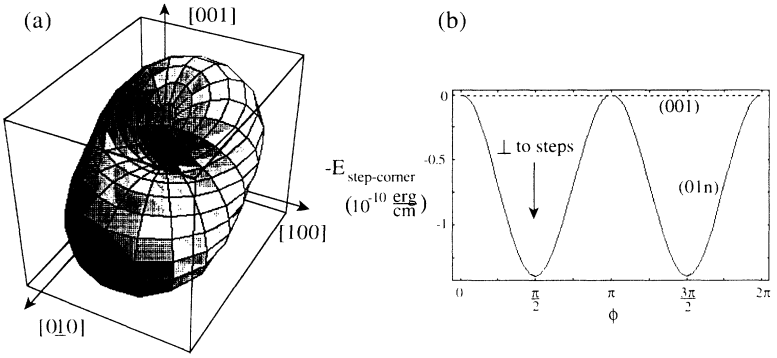


FIG. 14. (a) Anisotropy energy surface for a step-corner site in a bcc Fe (01$n$) film. (b) In-plane anisotropy for (001) and (0 1 14) planes through this surface. (001) anisotropy is shown in a dotted line, (0 1 14) anisotropy is in a solid line. The surface steps are along [100], defined by $\phi=0,\pi$.

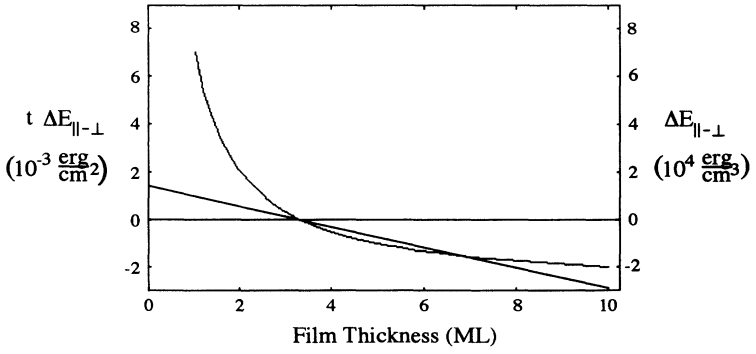


FIG. 15. Calculated uniaxial anisotropy in Fe/W(0 1 14) films as a function of film thickness. The straight line is the anisotropy energy times the film thickness (left scale), while the curve is the anisotropy energy (right scale). At 3.5 ML of Fe, the easy axis changes from perpendicular to the steps to parallel to the steps.

(0 1 14) plane of the film, however, the anisotropy is uniaxial, as shown by the solid line. The in-plane easy axis dictated by the bulk contribution is parallel to the steps ($\phi=0,\pi$): $\Delta E_{\parallel\text{-}\perp,\text{bulk}}=-2.7\times10^{4}$ erg/cm$^3$ ($-2.2\times10^{-7}$ eV/atom).

The surface contribution to the anisotropy, as shown in Fig. 13, favors magnetization perpendicular to the film [$\Delta E_{\text{out of plane-in plane}}=-0.11$ erg/cm$^2$ ($-6.8\times10^{-5}$ eV/atom)]. However, we consider **M** to be confined in-plane, as experimentally observed,[8] due to the strong magnetostatic energy [$2\pi M_s^2\sim10^7$ erg/cm$^3$ ($10^{-4}$ eV/atom)]. For **M** in the (001) plane, there is no anisotropy. In the vicinal film plane, which is no longer orthogonal to a high symmetry axis, uniaxial magnetic anisotropy is predicted, as shown by the solid line. The surface contribution favors **M** perpendicular to the steps: $\Delta E_{\parallel\text{-}\perp,\text{surface}}=1.9\times10^{-4}$ erg/cm$^2$ ($1.1\times10^{-7}$ eV/atom).

As mentioned above, the step-edge contribution to anisotropy is zero because no additional bonds around this site are broken to create steps parallel to [100]. The step-corner contribution, shown in Fig. 14, produces no anisotropy in the (001) plane, but favors **M** perpendicular to the steps in the film plane: $\Delta E_{\parallel\text{-}\perp,\text{step corner}}=1.4\times10^{-10}$ erg/cm ($2.5\times10^{-6}$ eV/atom).

Step sites are more important for Fe/W(01$n$) than Co/Cu(11$n$) because anisotropy in the cobalt system can be explained qualitatively by a (1 1 13) cut through the bulk and surface contributions. In the Fe system, consideration of only the bulk and surface contributions predicts an easy axis parallel to the steps, not perpendicular as experimentally observed. Only upon consideration of the step-site anisotropy is the true orientation of the easy axis obtained. Another significant difference between the two systems is that in the Co/Cu(11$n$) films step-induced uniaxial anisotropy is predicted regardless of whether **M** lies in the film plane (11$n$) or in the plane of the terraces (001). However, in Fe/W(01$n$), step-induced anisotropy only appears in the (01$n$) plane of the film.

The bulk, surface and step-site contributions described above, and the bulk magnetocrystalline anisotropy energy, combined as in Eq. (5), yield a $\Delta E_{\parallel\text{-}\perp,\text{film}}$ for Fe/W(01$n$) of the form

$$\Delta E_{\parallel\text{-}\perp,\text{film}}=\left[-0.3+\frac{1.0}{t_{\text{ML}}}\right]\times10^{5}\ \text{erg/cm}^3\ . \tag{9}$$

In ultrathin films, the strength of the in-plane uniaxial anisotropy in Fe/W vicinal to (001) films is two orders of magnitude smaller than that predicted for the Co/Cu system. Because the two terms in Eq. (9) are of opposite sign, there is a thickness at which the easy axis is predicted to switch from perpendicular to the steps, to parallel to the steps. This thickness, as can be seen from the plot of Eq. (9) in Fig. 15, is approximately 3.5 monolayers of Fe.

## VII. DISCUSSION

The Néel model, modified to include the effects of strain in the film, has been used to analyze the anisotropy in stepped Co/Cu and Fe/W films. The model predicts the correct orientation for the easy axis in both systems, explaining why in one case it is parallel to the steps, while in the other it is perpendicular to the steps. The quantitative prediction of the strength of the anisotropy is in crude agreement with observation in the Co/Cu system, predicting anisotropies approximately five times greater than those measured at room temperature. In the Fe/W system, the predicted anisotropy is considerably weaker than that measured by Chen and Erskine.[8] However, the thickness range in which step-induced uniaxial anisotropy is predicted for both systems agrees well with experiment; and the data follow the theoretical dependence of anisotropy on thickness reasonably well.

As shown by Draaisma and de Jonge,[22] for small film thicknesses the demagnetization energy found when treating a magnetic film as a collection of discrete dipoles can differ from that calculated based on a continuum approach. In the fcc Co/Cu (1 1 13) films for which we have obtained experimental anisotropy results, the film thicknesses ($>2.5$ nm) are well beyond the range in which surface effects are significant, as shown in Fig. 3 of Ref. 22. We assume that the demagnetization effects of the one atom high surface steps are also insignificant at these thicknesses, and therefore use the continuum value $-2\pi M_s^2$ for the magnetostatic energy of our films. We note that in the case of the Fe/W(001) vicinal films,[8] which are of thicknesses less than 0.4 nm, the discrete dipole approach should be used in calculating the magnetostatic energy to get a more accurate description of the films' anisotropy.

The importance of the step sites for accurate calculation of the uniaxial anisotropy is revealed in different ways for the two systems. For Co/Cu(1 1 13), the step site anisotropy contributions are not required to predict **M** parallel to the steps, but they are required to get better quantitative agreement with the measured anisotropy and to predict the correct thickness range in which the uniaxial anisotropy will appear. For Fe/W(0 1 14), the bulk anisotropy predicts an easy axis parallel to the steps for **M** confined to the (0 1 14) plane. This is not observed. Consideration of the step-site anisotropy is required to predict the correct sense and thickness range of the observed anisotropy.

In addition to explaining the uniaxial anisotropy observed in magnetic films on vicinal surfaces, results from our modified Néel anisotropy model, as listed in Tables II, III, and IV demonstrate other significant features of thin film anisotropy. For example, the anisotropy effects due to broken symmetry at surfaces or steps are always much stronger than any anisotropy effects due to typical misfit strains because the value of $L(r_0)$ is at least one order of magnitude greater than $e_0(dL/dr)r_0$ and $e_0L(r_0)$. Strain effects become important only when the symmetry-breaking effects balance each other leaving only strain-dependent terms in the anisotropy energies as, for example, in the surface anisotropies for sc(111), sc(110), and bcc(001) surfaces.

The Néel model also indicates that the bulk and surface of a material do not necessarily respond to strain in the same way. For example, in fcc(001) films, the strain-dependent bulk anisotropy is equal to $-[6e_0L(r_0)+e_0(dL/dr)r_0]$, while the strain dependent

surface anisotropy is $-3e_0L(r_0)$. For very thin films ($\sim$3 ML), the first term in the bulk anisotropy is partially balanced by the surface anisotropy [recall that in Eq. (5) the surface term is multiplied by $-2/t_{\rm ML}$]. The magnetic response of the film to strain will then be dominated by the $e_0dL/drr_0$ term in the bulk anisotropy. In thicker films, the surface effects will become less important and the full bulk response, proportional to $-[6e_0L(r_0)+e_0(dL/dr)r_0]$ will govern the behavior of the film. The film thickness range for which the surface response dominates the behavior may be different than predicted by our model due to exchange coupling of the surface and bulk atoms, which we have not included.[23]

In certain cases, the strain-dependent coefficient in the anisotropy energy may even change sign as the film thickness is increased. For example, in Co/Cu(001) films the values of $L(r_0)$ and $(dL/dr)r_0$ are of opposite sign, with the magnitude of $(dL/dr)r_0$ being larger by a factor of nearly 4 (Table I). While the surface effects are significant, and balancing the first term of the bulk anisotropy $[-6e_0L(r_0)]$, the overall strain-dependent anisotropy will have a negative coefficient. However, as the thickness increases, the sign of the strain-dependent anisotropy becomes positive. The film's magnetic response to strain changes character with film thickness.

A final trend present in the anisotropy energies given in Tables II, III, and IV is that the surface anisotropy for all (111) and (001) surfaces has no $\phi$ dependence. The creation of such surfaces will only affect the $\theta$ dependence of the film anisotropy (i.e., whether the film prefers in-plane or perpendicular magnetization). The in-plane anisotropy will be governed by the bulk magnetocrystalline anisotropy energy. However, upon the creation of a (110) surface, the surface site does contribute to in-plane anisotropy.

## VIII. CONCLUSION

We have used the Néel model modified to include strain effects to calculate the anisotropy energies $E_{\rm bulk}$ and $E_{\rm surface}$ for sc, bcc, and fcc structures with low index surfaces, as well as $E_{\rm step\ edge}$ and $E_{\rm step\ corner}$ for fcc(001) and bcc(001) vicinal surfaces. Our analysis of the vicinal surfaces explains the observed anisotropy in stepped Co/Cu(1 1 13) films with an easy axis parallel to the steps and Fe/W(0 1 14) films with an easy axis perpendicular to the steps.

The results of the model indicate important features in the anisotropy behavior of ultrathin films. For example, strain-induced anisotropy is of secondary importance relative to anisotropy due to broken symmetry, such as that which occurs at surfaces and steps. Also, the response of the bulk and the surface to strain is not necessarily the same. In some cases, this difference can even lead to a change in sign of the strain-dependent anisotropy coefficient.

## ACKNOWLEDGMENTS

We would like to thank H. P. Oepen for introducing us to the rich magnetic effects at stepped surfaces and for helpful comments. D.S.C. would like to thank the ONR for financial support.

## APPENDIX: DERIVATION OF ANISOTROPY ENERGY

This derivation involves summing the anisotropy for a bulk site over all the atoms in the film. The anisotropy energy created when bonds are broken to create the surfaces of the film and the steps in the film are then subtracted from the bulk anisotropy. The parameters used in the derivation are defined in Table V. The volume of the film is

$$V_{\rm film}=HLW\ {\rm cm}^3$$

and the number of atoms in the film is given by

$$N_{\rm film}=(\rho\ {\rm atoms/cm}^3)(V_{\rm film}{\rm cm}^3)=\rho HLW\ {\rm atoms}\ ,$$

where $\rho$ is the atomic density. The bulk anisotropy energy for all atoms in the film is

$$\mathcal{E}_{\rm film}=E^{\rm atom}_{\rm bulk\ site}\rho HLW\ {\rm erg}\ ,$$

where $E^{\rm atom}_{\rm bulk\ site}$ is in units of erg/atom. We must now subtract the anisotropy energy due to broken bonds at the surface ($E^{\rm atom}_{\rm surface\ site}$ erg/atom) and the steps ($E^{\rm atom}_{\rm step\ edge}$, $E^{\rm atom}_{\rm step\ corner}$ both in erg/atom). The total number of surface atoms in the film is

$$\begin{aligned}N_{\rm surf}&=2(\rho\ {\rm atoms/cm}^3)(W\ {\rm cm})(1\ {\rm ML})\\&\quad\times(h\ {\rm cm/ML})(L\ {\rm cm})\\&=2\rho WhL\ {\rm atoms}\ .\end{aligned}$$

The factor of 2 is present in the above equation because the film has 2 surfaces: film/vacuum and film/substrate. We assume that the anisotropy is the same for both surfaces. Our assumption neglects the fact that although the Co does not polarize the Cu at the interface, the Cu may reduce the moment of the Co. To improve our calculation, this effect should be accounted for by using an appropriate interaction parameter between Co-Cu atoms.

TABLE V. Parameters used to calculate the number of bulk, surface, and step atoms.

| Parameter | Definition | Units |
|---|---|---|
| $H=n_hh$ | Film thickness | cm |
| $n_h$ | Number of monolayers in the film | ML |
| $h$ | Thickness of one monolayer | cm/ML |
| $L$ | Length of the film (measured parallel to the steps) | cm |
| $W=n_ww$ | Width of the film (measured perpendicular to the steps) | cm |
| $n_w$ | Number of atoms in the width of the film | atoms |
| $w$ | Distance between atoms (measured perpendicular to the steps) | cm/atom |

However, we have no measure of this parameter. For systems such as Co/Pd,[1] the magnetic interaction between the Co and Pd at the film/substrate interface should result in a different surface anisotropy than that at the vacuum/film interface.

The number of step atoms is just a fraction of surface atoms which occur at the edges of the terraces. This number is obtained by dividing $N_{\text{surf}}$ by $d_A$, the number of atoms in one terrace width:

$$N_{\text{step}} = N_{\text{surf}}/d_A = 2\rho WhL/d_A \text{ atoms} .$$

The anisotropy energy of the film is then

$$\mathcal{E}_{\text{film}} = \rho WHLE^{\text{atom}}_{\text{bulk site}} - 2\rho WhLE^{\text{atom}}_{\text{surface site}} - 2\rho WhL\frac{(E^{\text{atom}}_{\text{step edge site}} + E^{\text{atom}}_{\text{step corner site}})}{d_A} \text{ erg} .$$

The energy per volume is

$$E_{\text{film}} = \frac{\mathcal{E}_{\text{film}}}{WHL} = E^{\text{atom}}_{\text{bulk site}}\rho - 2\rho\frac{E^{\text{atom}}_{\text{surface site}}}{n_h} - 2\rho\frac{(E^{\text{atom}}_{\text{step edge site}} + E^{\text{atom}}_{\text{step corner site}})}{n_h d_A} \text{ erg/cm}^3 .$$

If we write this in terms of $E_{\text{bulk}}$ energy/volume, $E_{\text{surface}}$ energy/area, $E_{\text{step edge}}$ energy/length, $E_{\text{step corner}}$ energy/length, $t$ the film thickness, and $d$ the terrace width, we obtain Eq. (5):

$$E_{\text{film}} = E_{\text{bulk}} - 2\frac{E_{\text{surface}}}{t} - 2\frac{(E_{\text{step edge}} + E_{\text{step corner}})}{td} \text{ erg/cm}^3 .$$


[1] R. H. Victora and J. M. MacLaren, Phys. Rev. B **47**, 11 583 (1993).

[2] G. Bochi, C. A. Ballentine, H. E. Inglefield, S. S. Bogomolov, C. V. Thompson, and R. C. O'Handley, in *Magnetic Ultrathin Films: Multilayers and Surfaces/Interfaces and Characterization,* edited by B. T. Jonker, S. A. Chambers, R. F. C. Farrow, C. Chappert, R. Clarke, W. J. M. de Jonge, T. Egami, P. Grünberg, K. M. Krishnan, E. E. Marinero, C. Rau, and S. Tsunashima, MRS Symposia Proceedings No. 313 (Materials Research Society, Pittsburgh, 1993), p. 309.

[3] C. Chappert and P. Bruno, J. Appl. Phys. **64**, 5736 (1988).

[4] R. C. O'Handley and S. W. Sun, in *Magnetic Thin Films, Multilayers, and Surfaces,* edited by S. S. P. Parkin, MRS Symposia Proceedings No. 231 (Materials Research Society, Pittsburgh, 1991), p. 485.

[5] M. Albrecht, T. Furubayashi, M. Przybylski, J. Korecki, and U. Gradmann, J. Magn. Magn. Mater. **113**, 207 (1992).

[6] A. Berger, U. Linke, and H. P. Oepen, Phys. Rev. Lett. **68**, 839 (1992).

[7] P. Krams, F. Lauks, R. L. Stamps, B. Hillebrands, G. Guntherodt, and H. P. Oepen, J. Magn. Magn. Mater. **121**, 483 (1993).

[8] J. Chen and J. Erskine, Phys. Rev. Lett. **68**, 1212 (1992).

[9] C. A. Ballentine, R. L. Fink, J. Araya-Pochet, and J. L. Erskine, Appl. Phys. A **49**, 459 (1989); B. Heinrich, K. B. Urguhart, A. S. Arrott, J. F. Cochran, K. Myrtle, and S. T. Purcell, Phys. Rev. Lett. **59**, 1756 (1987); N. C. Koon, B. T. Jonker, F. A. Volkening, J. J. Krebs, and G. A. Prinz, *ibid.* **59**, 2463 (1987).

[10] D. P. Pappas, K.-P. Kamper, B. P. Miller, H. Hopster, D. E. Fowler, A. C. Luntz, C. R. Brundle, and Z.-X. Shen, J. Appl. Phys. **69**, 5209 (1991); R. Allenspach and A. Bischof, Phys. Rev. Lett. **69**, 3385 (1992); C. Liu, E. R. Moog, and S. D. Bader, *ibid.* **60**, 2422 (1988); D. P. Pappas, K.-P. Kamper, and H. Hopster, *ibid.* **64**, 3179 (1990).

[11] L. Néel, J. Phys. Radium **15**, 225 (1954).

[12] U. Gradmann, J. Magn. Magn. Mater. **54-57**, 733 (1986).

[13] H. P. Oepen, C. M. Schneider, D. S. Chuang, C. A. Ballentine, and R. C. O'Handley, J. Appl. Phys. **73**, 6186 (1993).

[14] J. Lapujoulade, J. Perreau, and A. Kara, Surf. Sci. **129**, 59 (1983).

[15] H. L. Davis, J. B. Hannon, K. B. Ray, and E. W. Plummer, Phys. Rev. Lett. **68**, 2632 (1992).

[16] F. C. Franck and J. H. vander Merwe, Proc. R. Soc. London Ser. A **198**, 216 (1949).

[17] S. Chikazumi, *Physics of Magnetism* (Krieger, Florida, 1986), p. 168.

[18] H. Fujiwara, H. Kadomatsu, and T. Tokaunaga, J. Magn. Magn. Mater. **31-34**, 809 (1983).

[19] B. D. Cullity, *Introduction to Magnetic Materials* (Addison-Wesley, Phillipines, 1972), Chap. 8.

[20] H. P. Oepen, A. Berger, C. M. Schneider, T. Reul, and J. Kirschner, J. Magn. Magn. Mater. **121**, 490 (1993).

[21] D. S. Chuang, C. A. Ballentine, and R. C. O'Handley (unpublished).

[22] H. J. G. Draaisma and J. M. de Jonge, J. Appl. Phys. **64**, 3610 (1988).

[23] R. C. O'Handley and J. P. Woods, Phys. Rev. B **42**, 6568 (1990).

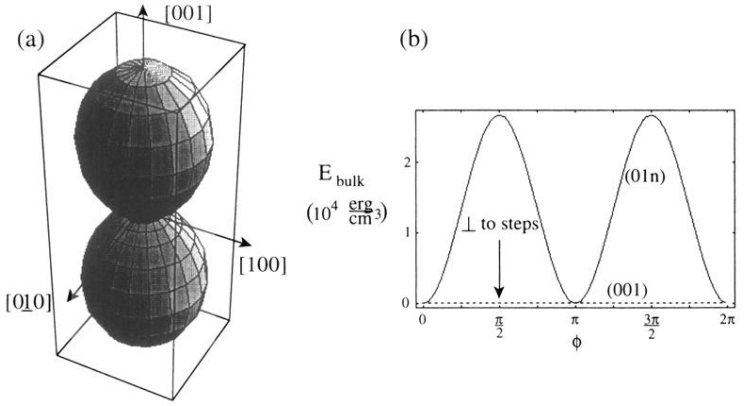


FIG. 12. (a) Anisotropy energy surface for a bulk site in a bcc Fe $(01n)$ film, and (b) in-plane anisotropy for (001) and (0 1 14) planes through this surface. (001) anisotropy is shown as a dotted line, (0 1 14) anisotropy as a solid line. The surface steps are along [100], defined by $\phi=0,\pi$.

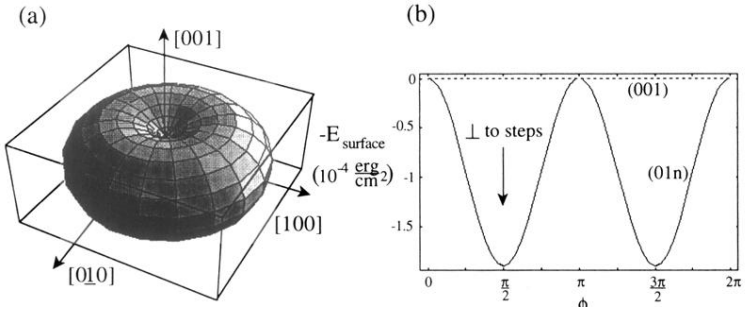


FIG. 13. (a) Anisotropy energy surface for a surface site in a bcc Fe $(01n)$ film. (b) In-plane anisotropy for (001) and (0 1 14) planes through this surface. (001) anisotropy is shown in a dotted line, (0 1 14) anisotropy is in a solid line. The surface steps are along [100], defined by $\phi=0,\pi$.

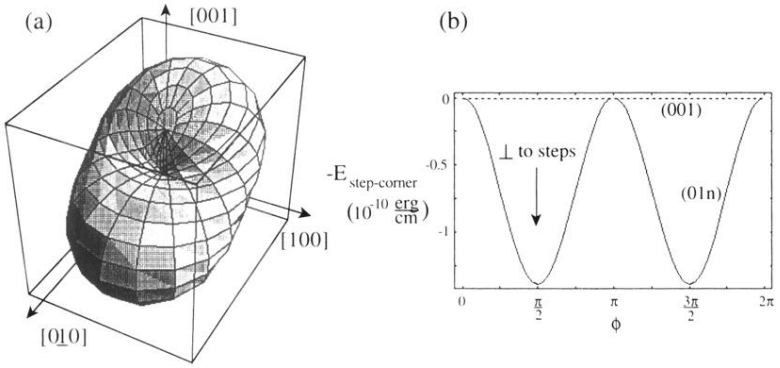


FIG. 14. (a) Anisotropy energy surface for a step-corner site in a bcc Fe $(01n)$ film. (b) In-plane anisotropy for (001) and (0 1 14) planes through this surface. (001) anisotropy is shown in a dotted line, (0 1 14) anisotropy is in a solid line. The surface steps are along [100], defined by $\phi=0,\pi$.

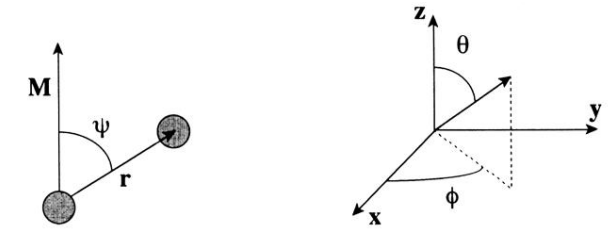


FIG. 2. (a) The angle $\psi$ between $\mathbf{M}_s$ and the bond axis, $\mathbf{r}$. (b) $\theta$ and $\phi$, the angles used to define the direction of a vector (e.g., $\mathbf{M}_s$) with respect to the coordinate axes.

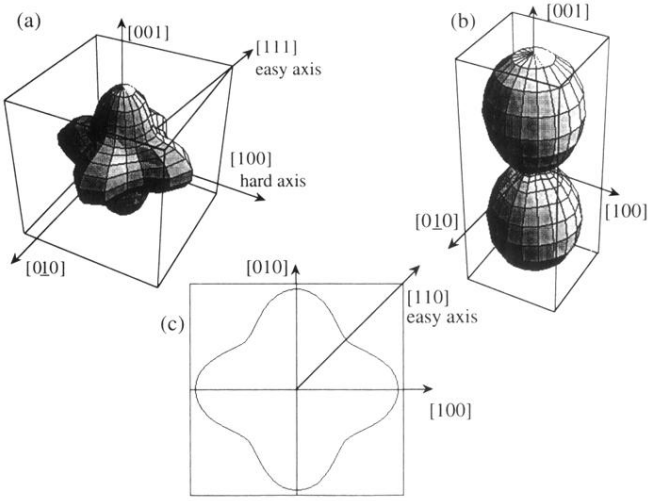


FIG. 4. (a) Anisotropy energy surface for unstrained fcc Co bulk. (b) Anisotropy surface energy for fcc Co bulk strained by the 1.9% misfit between Co and Cu induced by epitaxial growth on Cu. (c) An (001) cut through the strained bulk's energy surface showing the presence of fourfold anisotropy in the (001) plane.

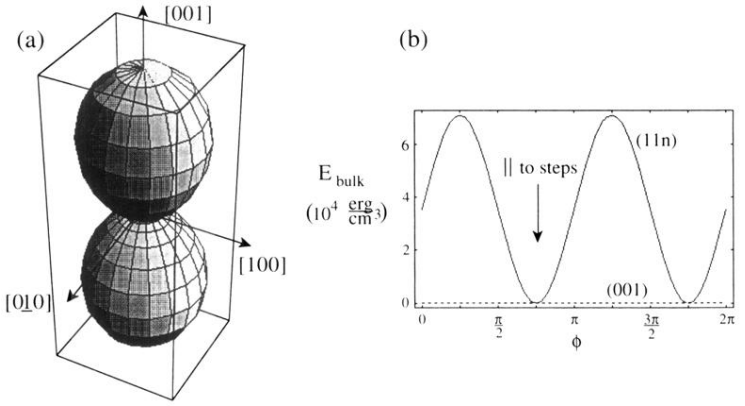


FIG. 5. (a) Anisotropy energy surface for a bulk site in a fcc Co(11$n$) film. (b) In-plane anisotropy for (001) and (1 1 13) planes through this energy surface. (001) anisotropy is shown as a dotted line, (1 1 13) anisotropy as a solid line. The surface steps are along [1$\underline{1}$0], defined by $\phi = 3\pi/4, 7\pi/4$.

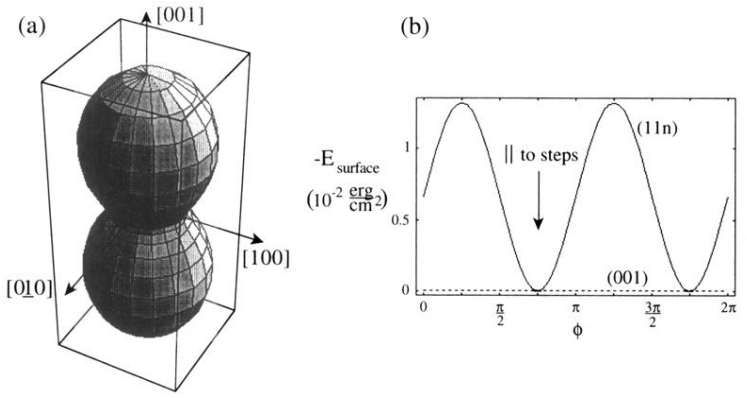


FIG. 6. (a) Anisotropy energy surface for the surface site in a fcc Co(11$n$) film. (b) In-plane anisotropy for (001) and (1 1 13) planes through this surface. (001) anisotropy is shown as a dotted line, (1 1 13) anisotropy as a solid line. The surface steps are along [1$\underline{1}$0], defined by $\phi = 3\pi/4, 7\pi/4$.

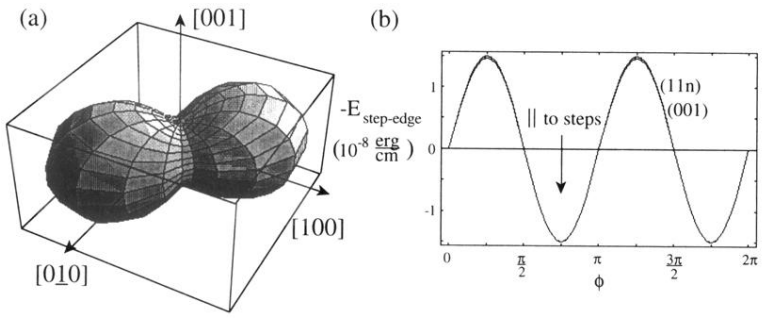


FIG. 7. (a) Anisotropy energy surface for the step-edge site in a fcc Co(11$n$) film. (b) In-plane anisotropy for (001) and (1 1 13) planes through this surface. (001) anisotropy is shown as a dotted line, (1 1 13) anisotropy as a solid line. The surface steps are along [1$\underline{1}$0], defined by $\phi = 3\pi/4, 7\pi/4$.

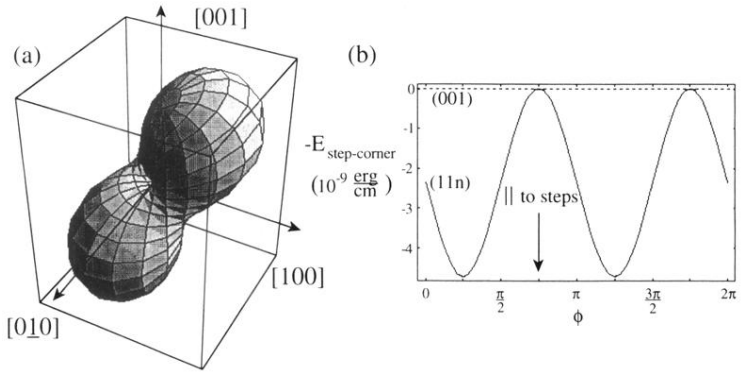


FIG. 8. (a) Anisotropy energy surface for the step-corner site in a fcc Co(11$n$) film. (b) In-plane anisotropy for (001) and (1 1 13) planes through this surface. (001) anisotropy is shown in a dotted line, (1 1 13) anisotropy is in a solid line. The surface steps are along [1$\underline{1}$0], defined by $\phi = 3\pi/4, 7\pi/4$.